Chemical Science

Accepted Manuscript

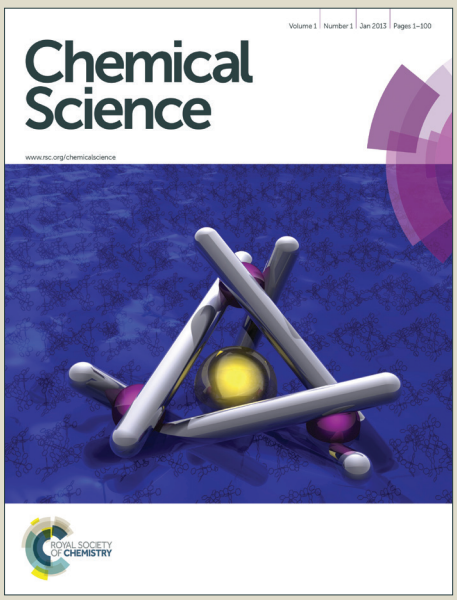

ROYAL SOCIETY OF CHEMISTRY

www.rsc.org/chemicalscience

Chemical Sciences

RSCPublishing

EDGE ARTICLE

N_2O reduction at a dissymmetric $\{Cu_2S\}$-containing mixed-valent center.

Cite this: DOI: 10.1039/x0xx00000x

Charlène Esmieu,[a,b,c] Maylis Orio,[d] Stéphane Torelli,[*a,b,c] Laurent Le Pape, [a,b,c] Jacques Pécaut,[b,e,f] Colette Lebrun[b,e,f] and Stéphane Ménage[a,b,c]

Received 00th January 2012,
Accepted 00th January 2012

DOI: 10.1039/x0xx00000x

www.rsc.org/

Through our bio-inspired approach toward replicating Nitrous Oxide reductase (N_2Or) activity, treatment of the $\mathbf{L^{Me(MAM)S\text{-}S}}$ ligand with $[Cu(CH_3CN)_4](OTf)$ (OTf = trifluoromethanesulfonate ion) leads to the isolation of a new dissymmetric mixed-valent (MV) dicopper (II,I) **[2.(H$_2$O)(OTf)]$^+$** containing a $\{Cu_2S\}$ core with labile triflate and water molecules at the copper centers. Whilst **[2.(H$_2$O)(OTf)]$^+$** is prone to ligand exchange under particular conditions, a raft of spectroscopic investigations, combined with theoretical calculations demonstrate that its structure is retained in acetone solution. Compared to our previously reported inactive parent complex **[1]** (*Angew. Chem. Int. Ed.* **2010**, *49* (44), 8249-8252) featuring a symmetric and saturated coordination sphere (N and S atoms from the ligand), **[2.(H$_2$O)(OTf)]$^+$** is reactive towards nitrous oxide in acetone. Spectroscopic and theoretical studies combined with kinetic measurements show that exchangeable positions are required for N_2O interaction. The isolation of the final product and its characterization by X-Ray crystallography as a doubly bridged (μ-thiophenolato)(μ-hydroxo) dicopper (II) species **[3.(μ-OH)(OTf)$_2$]** which helps to support the proposed reaction pathway. Implications for N_2Or mechanism are discussed.

Introduction

Alternatives for decreasing or at least limiting the effect of pollutants on the environment are nowadays of crucial interest. Among them, nitrous oxide (N_2O) has recently emerged as a major target since it is both a potent greenhouse agent (with a global warming potential more than 300 times higher than CO_2[1]) and an ozone-depleting gas.[2] N_2O is generated by abiotic processes such as those found in hypersaline ponds,[3] but is mainly a by-product of bacterial nitrification and denitrification respiratory pathways.

[a] *CNRS, UMR 5249, Laboratoire de Chimie et Biologie des Métaux, F-38054 Grenoble Cedex 9, France. E-mail : stephane.torelli@cea.fr*

[b] *Univ. Grenoble Alpes, F-38041 Grenoble Cedex 9, France.*

[c] *CEA-Grenoble, DSV/iRTSV, Laboratoire de Chimie et Biologie des Métaux, F-38054 Grenoble Cedex 9, France.*

[d] *Laboratoire de Spectrochimie Infrarouge et Raman, Bâtiment C5 - UMR CNRS 8516, Université des Sciences et Technologies de Lille, F-59655 Villeneuve d'Ascq Cedex, France.*

[e] *CNRS, UMR_E 3, F-38054 Grenoble Cedex 9, France*

[f] *CEA-Grenoble, INAC, Service de Chimie Inorganique et Biologique, F-38054 Grenoble Cedex 9, France.*

† Electronic supplementary information (ESI) available: Experimental section; synthesis, characterization, kinetics, temperature dependent NMR, electrochemistry and DFT details. CCDC reference number for **(C)**, **(D)**, **[2.(H$_2$O)(OTf]$^+$** and **[3.(μ-OH)(OTf)$_2$]**: 948576, 948576, 948574 and 948577, respectively.

Its accumulation is significantly enhanced by extensive fertilization in modern agriculture and the consequence is a disturbance of the global nitrogen cycle. Despite its inertness, N_2O reduction is thermodynamically favorable ($N_2O + 2H^+ + 2e^- \rightarrow N_2 + H_2O$, $E° = 1.35V$ at pH 7.0) and its activation consequently attractive in order to propose efficient sequestration or degradation systems.[4] Oxidation reactions with O-atom transfer from N_2O onto a substrate with release of $N_2(g)$ could be achieved.[5] However, few catalytic metal based-systems active under mild conditions have been reported so far.[6] The determination of factors that control the inherent reduction of N_2O by a metal is of critical importance for their design.

In Nature, N_2O is reduced by a copper-containing metalloenzyme called nitrous oxide reductase (N_2Or) during the last step of bacterial denitrification to dinitrogen and water.[7] Until 2011, based on spectroscopic,[8] theoretical,[9] and X-Ray crystallography data,[10] it was believed that the active site consisted of a unique tetranuclear copper site with a μ_4-bridging sulfide ligand and an extra solvent-derived molecule coordinated at the edge of the copper cluster (known as Cu_Z^*). This edge part was proposed to be the location of N_2O binding (Cu_I-Cu_{IV}, Fig. **1**, left). The 1-hole ($3Cu^I1Cu^{II}$) resting state undergoes slow reductive activation in presence of methyl viologen to access a fully reduced ($4Cu^I$) active state. However, upon purification under anaerobic conditions, a different form

has recently been identified by X-Ray crystallography. The active site, denoted Cu_Z, possesses a sulfide ligand at the Cu_I-Cu_{IV} edge (Fig. **1**, right).[11] A recent detailed comparative study of the reactivity of both active sites indicates that 1-hole Cu_Z reacts with N_2O at a very slow rate, and that the fully reduced Cu_Z^* is catalytically active at a higher rate.[12]

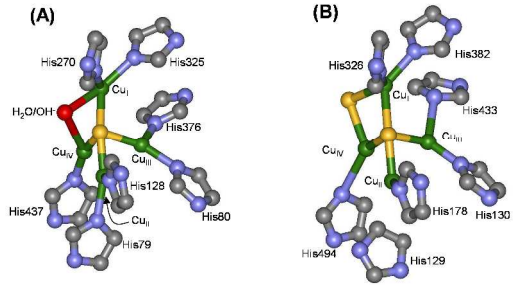

Fig. 1 Representations of the Cu_Z centers in *P. Denitrificans* (left, PDB ID 1FWX) and purple *P. Stuzeri* (right, PDB ID 3SBQ).

The mechanism of N_2O reduction is still under debate, with a μ-1,3-bent coordination mode at two copper ions previously proposed.[13] However, a recent *in-crystallo* study showed that N_2O could also interact with three Cu centers and the two bridging sulfur atoms.[14] It is proposed that the electrons needed for reduction would come from the Cu_A site located in close proximity to the Cu_Z. Given these data, the interaction between the active site and N_2O, along with the redox role of the copper centers, and consequently the reaction mechanism, remain unclear. Through model compounds, chemists have investigated the field by preparing copper-sulfur assemblies[15] with the aim at elucidating the reaction mechanism and at proposing alternative systems for N_2O remediation. The unique example of bio-inspired N_2Or reactivity has been reported by Tolman and co-workers, and consists of a trinuclear mixed-valent (MV) $[L_3Cu_3S_2](SbF_6)_2$ complex.[16]

Spurred by our bio-inspired approach toward replicating N_2Or activity, we reported in a previous paper the full characterization of a dinuclear MV complex (**[1]**, Chart **1**) containing a $\{Cu_2S\}$ core as a minimal structural motif of the Cu_Z center. **[1]** was unfortunately unreactive towards N_2O, presumably due to the poor ligating ability of the substrate and the saturated copper coordination sphere**.** On this basis, it was reasoned that a new generation of complexes containing exchangeable position(s) at the metal center(s) would allow for at least N_2O interaction. The strategy was to modify the $\mathbf{L^{Me(BPA)S\text{-}S}}$ ligand by replacing two methylpyridine arms with methyl groups (Chart **1**).

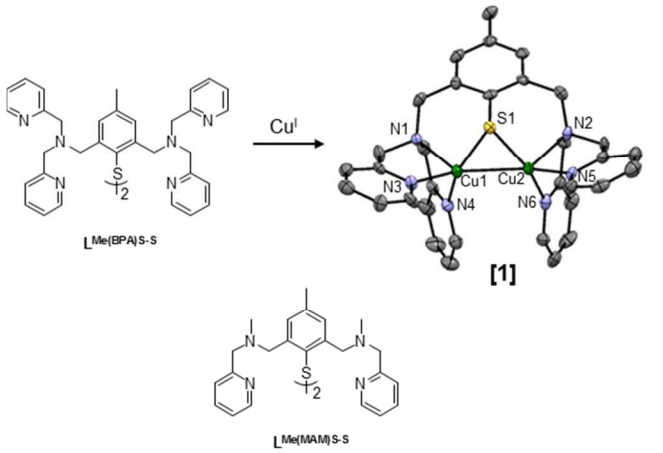

Chart 1. (Top) Preparation of the previously reported complex **[1]** and (bottom) structure of the targeted $L^{Me(MAM)S\text{-}S}$ ligand for this work.

Herein, we report the preparation and characterization of a new MV compound, $\mathbf{[2.(H_2O)(OTf)]^+}$, isolated from the reductive cleavage of the $\mathbf{L^{Me(MAM)S\text{-}S}}$ ligand by $[Cu(CH_3CN)_4](OTf)$. Solution studies show that while the structure of $\mathbf{[2.(H_2O)(OTf)]^+}$ is maintained in solution, the complex is prone to ligand exchange processes. We also demonstrate that $\mathbf{[2.(H_2O)(OTf)]^+}$ represents the only example, reported so far, of a dinuclear dissymmetric copper MV complex capable of N_2O reduction. A combination of mechanistic and theoretical studies suggests an interaction between N_2O and the title complex during the reaction pathway. Isolation of the reaction product as a dinuclear μ-hydroxo copper complex $\mathbf{[3.(\mu\text{-}OH)(OTf)_2]}$ illustrates the relevance of this extra ligand in the copper coordination sphere of N_2Or. A few of the copper complex properties for a rationale of N_2O activation/reduction are then highlighted. Implications on N_2Or mechanism are also discussed.

Results and discussion

Synthesis and solid-state characterization of $\mathbf{[2.(H_2O)(OTf)]^+}$.

The preparation of the $\mathbf{L^{Me(MAM)S\text{-}S}}$ ligand (supporting information) differs from our previously reported procedure for $\mathbf{L^{Me(BPA)S\text{-}S}}$. The new synthetic route (Scheme **1**) provides an alternative, in which the pivotal tetrachloro intermediate **(D)** can be further functionalized by various amines under mild conditions. Reduction of the S-thiocarbamate **(A)** with lithium aluminum hydride yielded the free thiophenol **(B)** that was unstable under aerobic conditions. The corresponding disulfide tetraol **(C)** (Tables S1, S2 and Fig. S3) was obtained using Et_3N/O_2/THF conditions. Chlorination allowed the transformation to the tetrachlorinated analogue **(D)** (Tables S1, S3 Fig. S3) and subsequent nucleophilc substitution with 2-[(methylamino)methyl]pyridine finally gave the targeted $\mathbf{L^{Me(MAM)S\text{-}S}}$ ligand (global yield 7 %).

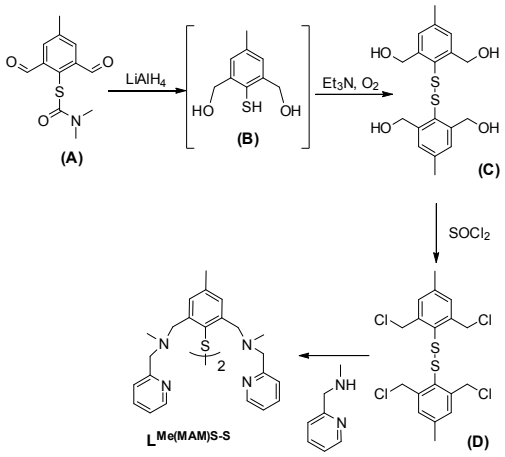

Scheme 1

Like $\mathbf{L^{Me(BPA)S-S}}$, combination of the $\mathbf{L^{Me(MAM)S-S}}$ ligand with 4 eq. of $[Cu(CH_3CN)_4](OTf)$ in acetone under anaerobic conditions resulted in the isolation of an intensely colored violet powder. Suitable X-ray diffraction single crystals were obtained upon layering pentane onto an acetone solution of the complex. The solid-state structure of **[2.(H_2O)(OTf)](OTf)** (the corresponding complex will herein be abbreviated to **[2.(H_2O)(OTf)]**$^+$) reveals a unique example of a $\{Cu_2S\}$ core bearing non-equivalent exogenous ligands (Fig. **2**). Selected bond lengths and angles (in comparison with **[1]**) are listed in Table **1** (see also Tables S1 and S4 for additional crystallographic data).

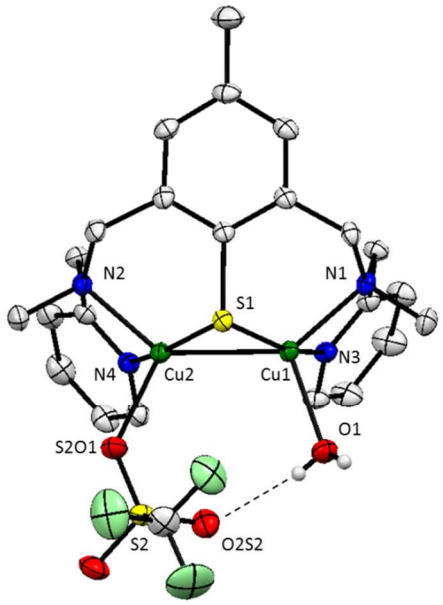

Fig. 2 Single-crystal X-ray structure of the monocationic unit of **[2.(H_2O)(OTf)]**$^+$ with thermal ellipsoids plotted at 50 % occupancy. Hydrogen atoms are omitted for clarity except for the coordinated water molecule.

Table 1. Selected Bond Distances (Å) and Angles (°) for **[2.(H_2O)(OTf)]**$^+$ and **[1]**.

[2.(H_2O)(OTf)]$^+$		**[1]**[17]	
Cu(1)-Cu(2)	2.5674(4)	Cu(1)-Cu(2)	2.576(13)
Cu(1)-S1	2.1806(5)	Cu(1)-S(1)	2.177(2)
Cu(1)-N(1)	2.0627(16)	Cu(1)-N(1)	2.127(7)
Cu(1)-N(3)	1.9774(16)	Cu(1)-N(3)	2.119(6)
Cu(1)-O(1)	2.1643(17)	Cu(1)-N(4)	1.98(7)
Cu(2)-S1	2.1686(5)	Cu(2)-N(2)	2.115(7)
Cu(2)-O(1)S(2)	2.2115(15)	Cu(2)-N(5)	2.124(7)
Cu(2)-N(2)	2.0737(16)	Cu(2)-N(6)	1.998(7)
Cu(2)-N(4)	1.9562(17)	Cu(2)- S(1)	2.193(2)
Cu(1)-S-Cu(2)	72.358(17)	Cu(1)-S-Cu(2)	71.53(9)
S-Cu(1)-Cu(2)	53.604(15)	S(1)-Cu(1)-Cu(2)	53.69(4)
S-Cu(2)-Cu(1)	54.038(15)	S-Cu(2)-Cu(1)	54.78(6)

Like **[1]**, the monocationic unit is consistent with a MV state. The structure shows a dissymmetric dinuclear moiety, each copper ion being pentacoordinated with two nitrogen and one sulfur atoms from the ligand, one Cu and an extra position occupied either by an oxygen from a water molecule or from a triflate anion. For the two metal centers, the geometry can be best described as distorted tetragonal with τ values for Cu1 and Cu2 of 0.29 and 0.36 respectively.[18] The main common feature for both complexes is the presence of a Cu-Cu bond (confirmed by theoretical calculations, see below). By comparison with the literature, these Cu-Cu distances remain the largest ever reported (usually, Cu-Cu bonds range between 2.39 and 2.45 Å[19]). Interestingly, differences in the metal coordination sphere between **[1]** and **[2.(H_2O)(OTf)]**$^+$ (N pyridines atoms replaced by O from water and triflate) have limited effects on the overall bond lengths since only the tripodal N-Cu distances are affected. A relatively short stabilizing hydrogen bond between the coordinated triflate and water molecules (S_2O_2…H-O1 = 2.132 Å, S_2O_2-H-O1 = 137°) is also present within the unit, that may account for the stabilization of the structure. The Cu-OSO_2CF_3 distance is intermediate compared to others reported in the literature for copper centers being at the +I or +II oxidation states[20] or to **[3.(μ-OH)($OTf)_2$]** *(vide infra)*. Consequently, the redox states of both copper in **[2.(H_2O)(OTf)]**$^+$ are not crystallographically distinguishable.

The electronic structure of **[2.(H_2O)(OTf)]**$^+$ was then investigated by theoretical methods. The DFT-optimized geometry (Table S5, Fig. S4) compares well with the crystallographic data. Mülliken spin population analysis indicates an equally distributed spin density between the copper and sulfur atoms with positive spin populations found at Cu_1 (0.27), Cu_2 (0.27) and S (0.23). The spin density of the Cu and S atoms accounts for 77 % of the total spin density and the remaining 23 % are spread over the pyridine rings (Fig. S5). Not surprisingly, the Singly Occupied Molecular Orbital (SOMO) of **[2.(H_2O)(OTf)]**$^+$ displays 57 % Cu character and 20 % S character featuring the σ antibonding interaction between the Cu $3d_z^2$ orbitals and the S $3p_x$ orbital (Fig. S5). Contribution of the S atom in the SOMO suggests a non-negligible degree of covalency for the Cu-S bond. These results evidence a class III mixed-valence state for **[2.(H_2O)(OTf)]**$^+$ which is further confirmed by Natural Population Analysis

(NPA). The NPA analysis shows two identically positive copper centers (0.97 and 1.00, respectively) and a partially negative sulfur (-0.25), matching the expectations for a fully delocalized $Cu^{+1.5}Cu^{+1.5}$ state in **[2.(H$_2$O)(OTf)]$^+$**. The relevance of the Cu-Cu bond was investigated using Natural Bond Order (NBO) analysis. The Wiberg bond index obtained in **[2.(H$_2$O)(OTf)]$^+$** has a similar value compared to the one determined for **[1]** (0.39 against 0.40, respectively, Table S6). This value reveals that the Cu-Cu bond features a character intermediate between covalent and ionic which suggests that the two copper ions are linked together by one three-electron bond (odd electron bond). An unequivocal representation of the Cu-Cu bond extracted from the NBO analyses indicates a σ (sd/sd) overlap between the two metal centers. The corresponding orbital is depicted in Fig **3**, highlighting the hydrogen bond between the coordinated triflate and water molecules (Fig **3**, right, dotted line).

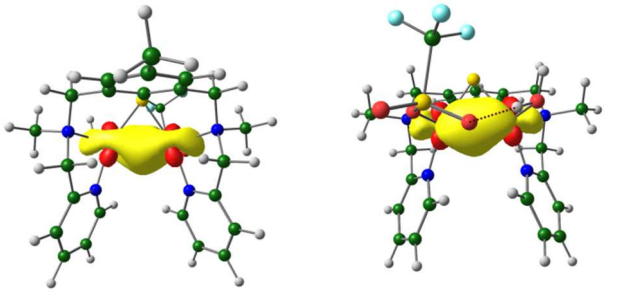

Fig 3. Selected views for the occupied natural orbital relevant to the Cu-Cu bond in **[2.(H$_2$O)(OTf)]$^+$**.

Solution studies of [2.(H$_2$O)(OTf)]$^+$.

As we wish to investigate the reactivity of **[2.(H$_2$O)(OTf)]$^+$** towards N_2O, whether or not its structure is retained in solution needs to be clarified. All the following experiments were performed using crystalline **[2.(H$_2$O)(OTf)]$^+$**, acetone (Ac) as solvent (acetone was chosen because of its low coordinating ability for copper centers) and under inert atmosphere unless otherwise specified. Upon dissolution, due to possible ligand exchange processes, several species have to be considered (Chart **2**). **[2.(H$_2$O)(OTf)]$^+$** is the X-Ray isolated material, **[2.(H$_2$O)$_2$]$^{2+}$** has two coordinated water molecules (the extra one coming from the solvent), and **[2.(OTf)$_2$]** two triflate ions. The coordinating acetone counterparts are also of interest. The electrospray ionization (ESI) mass spectrum of **[2.(H$_2$O)(OTf)]$^+$** in acetone (Fig. S6) displayed a prominent peak at m/z = 666.0 corresponding to a monocationic mono triflate-containing fragment $[L^{Me(MAM)S-} + 2Cu + 1OTf^-]^+$.

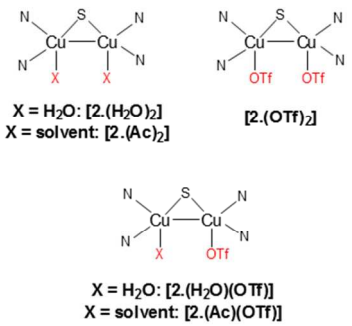

Chart 2. Possible speciation upon dissolution of **[2.(H$_2$O)(OTf)]$^+$** in acetone.

UV-Vis and near-IR Spectrophotometry. Spectra recorded for **[2.(H$_2$O)(OTf)]$^+$** in solid-state and in acetone are depicted in Fig. **4**. In solution, transitions are observed at 1254 nm (ε = 690 $M^{-1}.cm^{-1}$), 787 nm (ε = 735 $M^{-1}.cm^{-1}$), 479 (sh, ε = 525 $M^{-1}.cm^{-1}$) and 425 (sh, ε = 670 $M^{-1}.cm^{-1}$). The energy of the near-IR band is strongly solvent-dependent, and is in the same range as for **[1]** and other MV synthetic models (Table S7). These transitions are usually assigned to $\Psi \rightarrow \Psi^*$ transitions or Inter Valence Charge Transfer (IVCT) processes.[21] In strongly coupled systems like biological Cu_A, these features are observed in the visible region (780-810 nm).[22] The solid-state spectrum exhibits very broad peaks (1235 nm and 802 nm), but its resemblance to the solution spectrum suggests that the structure of **[2.(H$_2$O)(OTf)]$^+$** is maintained upon solvation.

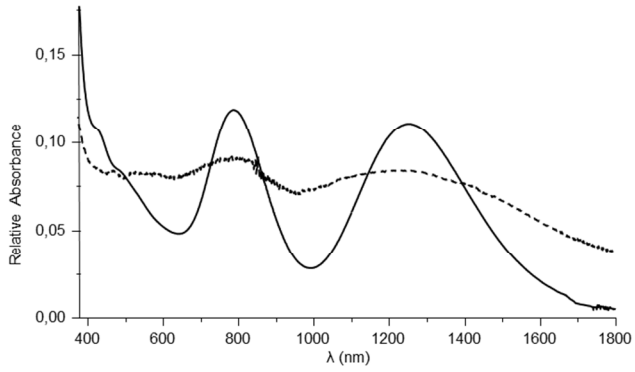

Fig. 4 Electronic absorption spectra of polycrystalline **[2.(H$_2$O)(OTf)]$^+$** in acetone (solid line) and in solid-state (dotted line). See the main text for λ_{max} and Table S7 for ε values and comparison with other MV systems.

Acid-base titration followed by UV-visible spectrophotometry then provided a mean to assess the presence of a coordinated water molecule. Addition of a non-coordinating organic base such as 1,4-diazabicyclo[2.2.2]octane (DABCO) into an acetone solution of polycrystalline **[2.(H$_2$O)(OTf)]$^+$** resulted in drastic changes of the starting material up to one molar equivalent (Fig. **5**). We observed the disappearance of the two main features of **[2.(H$_2$O)(OTf)]$^+$** concomitantly with the appearance of new shoulders at 775 nm (ε= 100 $M^{-1}.cm^{-1}$) and 570 nm (ε= 170 $M^{-1}.cm^{-1}$). ESI-MS analysis of the end product

shows the presence of a monocationic species, consistent with a hydroxo ligand within the complex ion before fragmentation (Fig. S7). This new species is oxygen sensitive and upon exposure to O_2, the final UV-visible spectrum is comparable to that of **[3.(μ-OH)(OTf)$_2$]** (Fig. S8, see also the reactivity section), re-enforcing the assignment of **[2.(H$_2$O)(OTf)]$^+$** as a MV complex. Moreover, this transformation is reversible with the addition of methanesulfonic acid (Fig. **5**, dotted line). Such spectroscopic data infers for coordination of one water molecule at the metals centers, that is deprotonated upon addition of the organic base. This result suggests that the structure of **[2.(H$_2$O)(OTf)]$^+$** is maintained in acetone solution. A plausible structure for this new species could be formulated as **[2.(OH)(OTf)]**, which is neutral in the MV state.

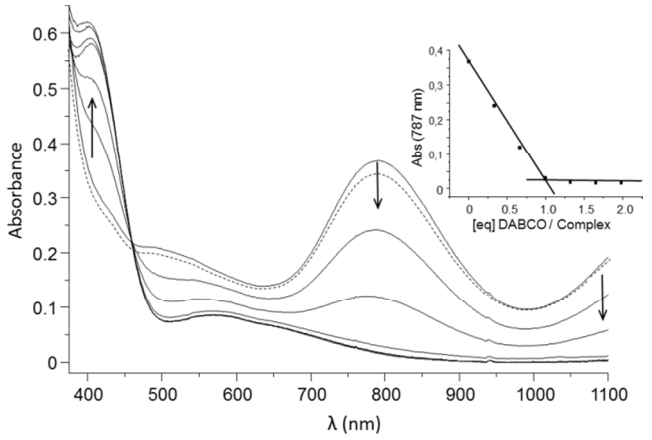

Fig 5. Changes in the UV-Vis spectrum of crystalline **[2.(H$_2$O)(OTf)]$^+$** (0.5 mM in acetone) upon progressive addition of DABCO (0 to 2 molar equiv.). The dotted line spectrum corresponds to the back-titration with methanesulfonic acid (1 molar equiv.).

Moreover, addition of excess triflate (NaOTf, 200 molar equiv.) to a solution of **[2.(H$_2$O)(OTf)]$^+$** is accompanied by slight but significant changes on the UV-Vis spectrum (Fig. S9), again indicating modifications at the metal centers, which suggests that the water molecule of **[2.(H$_2$O)(OTf)]$^+$** could be exchanged with one triflate to give **[2.(OTf)$_2$].** A similar behavior has been reported reported by Latour and co-workers. for ligand exchanges processes at a MV diiron compound.[23]

To fully assign the electronic features of the UV-Vis-NIR spectrum of **[2.(H$_2$O)(OTf)]$^+$**, TD-DFT calculations were performed in acetone as solvent on the DFT-optimized structure. The calculated electronic excitations (Fig. S10) are in good agreement with the experimental ones (1254 nm_{exp} / 1205 nm_{calc}, 787 nm_{exp} / 758 nm_{calc} and 425 nm_{exp} / 452 nm_{calc}). Based on the data predicted by TD-DFT, the main features of the experimental spectrum were assigned. The solvent-dependent near-IR band is attributed to $\Psi \rightarrow \Psi^*$ transitions (reminiscent of class III MV systems), as the contribution of both copper centers is identical for the donor and acceptor orbitals. The two other bands correspond to expected $N_{ligand} \rightarrow Cu$ and $S_{ligand} \rightarrow Cu$ LMCT transitions (425 nm and 787 nm respectively, Fig. S10 and Table S8).

^{19}F NMR spectroscopy

The presence of triflate ions in crystalline **[2.(H$_2$O)(OTf)]$^+$** allows the use of ^{19}F NMR as an additional tool solution studies. A unique broad peak at -73.30 ppm was observed at 298 K upon dissolution of **[2.(H$_2$O)(OTf)]$^+$** in acetone. A subsequent sharpening and shift (from -73.30 ppm to -79.60 ppm, Fig **6**) upon lowering the temperature was observed, suggesting a rapid solution exchange process compared to the NMR timescale. Interestingly, the 208 K peak lies in the region where diamagnetic (NaOTf), or non-coordinated triflates ([Cu(OTf)$_2$], Fig. S11) were detected in our experimental conditions. Using an internal reference, an integral value close to 6 (corresponding to two triflates) was obtained at room temperature; while a value of 3 (one triflate) was determined at 208 K. This result suggests that the loss of intensity is related to the existence of a highly paramagnetic triflate-containing species having too fast relaxation time to be observed at low temperature.

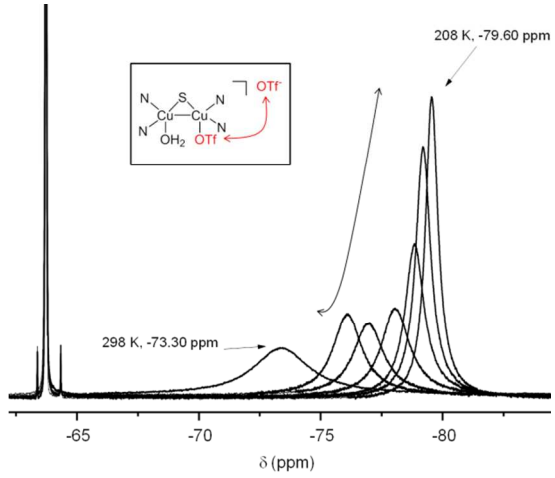

Fig 6. Temperature dependence of the ^{19}F NMR spectrum for polycrystalline **[2.(H$_2$O)(OTf)]$^+$** in d_6-acetone. Inset: postulated observed exchange. The peak at -63.73 ppm refers as the internal standard.

Consequently, we propose that the observed exchange is occurring between the triflate counter-ion and the coordinated one (Fig. **6**, inset). At low temperature, the observed signal mainly originates from the non-coordinated ion and is less subject to the metal paramagnetism while at room temperature the peak gets broader due to the effect of Cu paramagnetism on the electronic properties of both triflates. This assertion is supported by comparison of the temperature-dependence of the unique resonance for **[1]** (Fig. S12). By plotting the variation of the chemical shift as a function of the temperature for **[2.(H$_2$O)(OTf)]$^+$** displayed an exponential trend while a straight line behavior was obtained for **[1]**. For the later, as the metal coordination sphere is saturated, the trend accounts for non-coordinating triflates and is directly correlated to the temperature dependence of the paramagnetic susceptibility ($\Delta\delta$ = 2.40 ppm). The fact that a different behaviour is observed for **[2.(H$_2$O)(OTf)]$^+$** implies that another phenomenon is present on top of susceptibility variation, *i.e.* an exchange process

involving triflates(s) ions coordinated to the copper centers (Δδ = 6.30 ppm).

Electrochemical Studies.

To further corroborate the presence of an exchangeable position at the metal center, the electrochemical properties of polycrystalline **[2.(H$_2$O)(OTf)]$^+$** in acetone were investigated by cyclic voltammetry. Starting from the Open Circuit Potential, the CV curve of **[2.(H$_2$O)(OTf)]$^+$** (Fig. **11**, trace **(A)**) exhibited two prominent quasi-reversible waves. The first one (E_{pa1} = -40 mV, E_{pc1}= -180 mV, $E_{1/2}$ = -110 mV, ΔEp = 140 mV) is assigned to a Cu^ICu^I/Cu^ICu^{II} system and the second (E_{pa2} = 490 mV, E_{pc2}= 345 mV, $E_{1/2}$ = 417 mV, ΔEp = 145 mV) to a $Cu^{II}Cu^I/Cu^{II}Cu^{II}$ redox process. The large ΔEp values (compared to Fc^+/Fc in our experimental conditions, ΔEp = 85 mV) are consistent with highly energetic reorganization processes at the copper coordination spheres.

Upon deprotonation, the resulting new species exhibits two irreversible waves at E_{pa} = 16 mV and E_{pc} = -475 mV *vs* $Ag/AgNO_3$ (Fig. S13). This behavior differs from the starting material, confirming ligand modifications at the metal coordination sphere. In particular, the shift toward a lower E_{pa} value is consistent with the presence of more donating ligand(s) prone to stabilize Cu^{II}, *i.e* OH^-. Moreover, addition of a large excess of NaOTf (200 molar equiv., Fig. S14) caused a shift of the 417 mV signal to $E_{1/2}$ = 365 mV (ΔE = 52 mV) while the other redox system was less affected (ΔE = 20 mV). This result accounts for the influence of an exchange process reaction equilibrium on a "square scheme" framework involving successive oxidation states of the complex. Accordingly, the change in ligand selectivity induces the standard potential of the two couples to be different. In our case, addition of a ligand stronger than that of a water molecule into the solution causes the resulting MV system to become easier to oxidize, as expected. This again confirms that exchanges occur at the redox active centers and that it is possible to introduce an additional triflate molecule (in place of the water molecule) to give **[2.(OTf)$_2$]**. Consequently, the slight changes observed at the lower redox potential system is assigned to the Cu with the OTf ligand (Cu2 in the X-Ray structure) and the other to the Cu/H$_2$O counterpart (Cu1). Such a behavior is also exhibited in a mixed valent diiron complex involved in ligands exchange processes.[23] Finally, upon O_2 bubbling into either one of the above solutions, the resulting CV corresponds to that of **[3.(μ-OH)(OTf)$_2$]** (Fig **11**, trace **(C)**).

EPR Spectroscopy.

The EPR spectrum (Fig. 7) recorded at 10 K in acetone for polycrystalline **[2.(H$_2$O)(OTf)]$^+$** shows a seven lines pattern consistent with the presence of a fully delocalized mixed-valent dicopper system (2nI+1 = 7 with I = 3/2, n = 2 for S = 1/2=). This spectrum can be best simulated using parameters consistent with this observation (90 %, g = 2.137, 2.100, 2.028; ACu_1 = ACu_2 = 224, 40, 55 MHz), together with an extra mononuclear Cu^{II} species (10%, g = 2.272, 2.095, 2.006; ACu_3 =360, 0, 0 MHz) from O_2 contamination. The signal vanished above 40 K and no differences were observed as a function of power saturation. The observed g values compare well with the calculated ones (g = 2.118, 2.101, 2.034). As full delocalized systems are usually consistent with symmetrical complexes (see for example[19b, 19d-f, 24]), this result is rather surprising since **[2.(H$_2$O)(OTf)]$^+$** is not symmetrical. Minor modifications occurred upon addition of 200 molar equiv. of NaOTf (changes in intensity without altering either g or A values, Fig. S15), as observed by UV-Vis and electrochemistry. The introduction of an extra triflate ion (in place of the water molecule) has thus moderate effects on the EPR spectrum.

Conversely, addition of DABCO to the starting **[2.(H$_2$O)(OTf)]$^+$** complex revealed a localized MV state (upon exposure to air the signal vanished), with the EPR signature and parameters in agreement with a mononuclear Cu(II) species (Fig. S16).

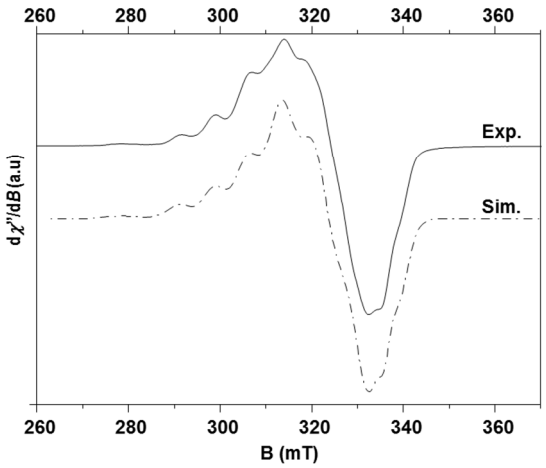

Fig. 7 X-band EPR spectrum (9.39 GHz) of **[2.(H$_2$O)(OTf)]$^+$** in acetone 0.14 mM at 10 K. Dotted line simulation with parameters given in the text.

To finalize the description of our system, we tried to evaluate the relative stability of the other dinuclear complexes possibly relevant in solution. Four species depending on the nature of the exchangeable ligand found in axial positions (water, triflate or acetone) were considered and electronic structure calculations were undertaken on DFT-optimized **[2.(H$_2$O)(OTf)]$^+$**, **[2.(OTf)$_2$]**, **[2.(H$_2$O)$_2$]$^{2+}$** and **[2.(Ac)$_2$]$^{2+}$** models. For energetic analysis, the total electronic energies of the complexes were shifted by subtracting from them the electronic energy of the corresponding optimized axial ligands. Consequently, the basis set superposition error was accounted for in the calculation of the final energies of the complexes. The calculated free energies for the four complexes in acetone predict **[2.(H$_2$O)(OTf)]+** to be lower in energy by 6.32, 7.50 and 10.06 kcal.mol^{-1} at 300 K when compared to **[2.(OTf)$_2$]**, **[2.(H$_2$O)$_2$]$^{2+}$** and **[2.(Ac)$_2$]$^{2+}$** (Chart 2, Fig. **8**), respectively. The results of these calculations are in good agreement with our experimental data, particularly the X-ray ones, with both predicting the same stable species.

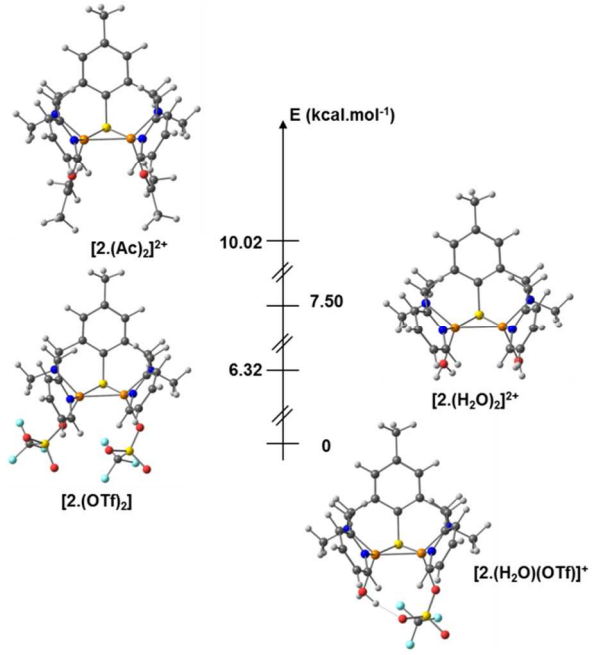

Fig. 8 Calculated relative energies for the possible relevant species in solution **[2.(H$_2$O)(OTf)]$^+$**, **[2.(OTf)$_2$]**, **[2.(H$_2$O)$_2$]$^{2+}$** and **[2.(Ac)$_2$]$^{2+}$**.

In combination, these spectroscopic data have established that ***[2.(H$_2$O)(OTf)]$^+$*** *is the predominant species in acetone solution. We suggest that its stability is related to the presence of the hydrogen bond between the triflate and the water molecule. A fast exchange between the coordinated water and the triflate ion may account for the observation of fully delocalized system. Upon deprotonation, a new* ***[2.(HO)(OTf)]*** *derivative with peculiar spectroscopic properties has been characterized.*

Reactivity toward N_2O and mechanistic studies.

When N_2O was bubbled into an acetone solution of **[2.(H$_2$O)(OTf)]$^+$**, under an Ar atmosphere and at room temperature, significant changes occurred on the UV-Vis spectrum, with the initial dark blue solution gradually turning to a pale green after 12 minutes (Fig. **9**).

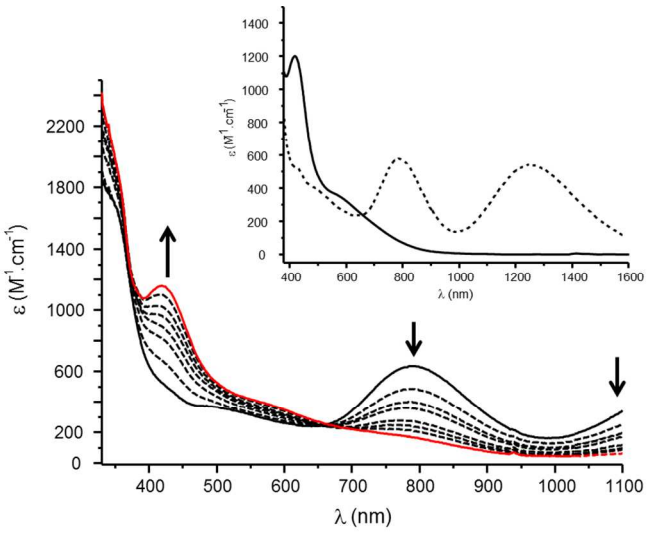

Fig. 9 Evolution of the UV-Vis spectrum recorded upon progressive N_2O bubbling (0 - 12 min) into a 0.67 mM acetone solution of **[2.(H$_2$O)(OTf)]$^+$** (black). The red line corresponds to the final spectrum. The inset shows the UV-Vis NIR spectra upon (dashed line) and after N_2O exposure (solid line, 12 min).

The spectrum of the starting material completely vanished with the appearance of new shoulders at 785 nm (sh, ε= 200 $M^{-1}.cm^{-1}$) and 572 nm (sh, ε= 380 $M^{-1}.cm^{-1}$) and a peak at 422 nm (ε= 1150 $M^{-1}.cm^{-1}$). The presence of an isosbestic point at 660 nm could indicate that the starting material is converted to the final species in a single step, or through an intermediate having no distinct features. The formation of an oxidized species becomes relevant since the spectrum is not further modified upon exposure to air. Monitoring the evolution of the EPR spectrum upon progressive N_2O bubbling showed the complete loss of the S=1/2 signal (Fig. S17) without the observation of distinct transient resonances. In addition, GC-MS analyses were carried out on the reaction headspace gas. After various control experiments (glove box atmosphere, **[2.(H$_2$O)(OTf)]$^+$** alone), clear evidence of N_2 release was observed only in presence of the title complex with N_2O (Fig. S18). The calculated N_2/O_2 ratio suggests that no O_2 contamination occurred during the experiment. ESI-MS experiments on the final reaction mixture reveals the presence of a monocationic molecular peak at m/z = 685.1 that is tentatively assigned to a dinuclear copper(II) complex with an extra hydroxide (Fig. S19). The chemical structure of the final product was then confirmed through isolation of single crystals suitable for X-ray diffraction, which were grown by dissolving the reaction product (green powder after evaporation) in acetone and layering with diisopropyl ether. The structure (Fig. **10**) shows the presence of a dinuclear entity in which the two copper centers are bridged by the sulfur atom from the ligand and by a hydroxo ion. The coordination sphere is completed by the nitrogen atoms from the ligand and by oxygen atoms from the triflate counter-ions.

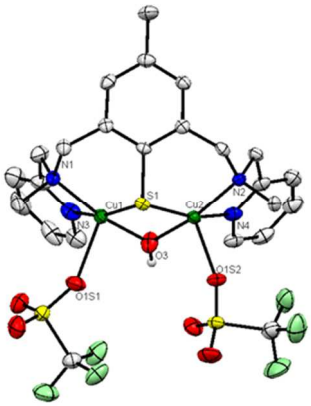

Fig. 10 Single-crystal X-ray structure of the neutral unit of **[3.(μ-OH)(OTf)$_2$]** with thermal ellipsoids plotted at 50% occupancy. Hydrogen atoms are omitted for clarity except for the coordinated hydroxo ligand. Selected bond lengths (Å) and angles (°): Cu1-Cu2, 2.9447(6); Cu1-S1, 2.3242(9); Cu2-S1, 2.3268(9); Cu1-N1, 2.027(3); Cu1-N3, 2.017(3); Cu2-N2, 2.056(3); Cu2-N4, 2.009(3); Cu1-O1S1, 2.313(3); Cu2-O1S2, 2.271(2); Cu1-O3H, 1.915(3); Cu2-O3H, 1.926(3); see table S9 for complete crystallographic data.

The Cu-Cu distance in **[3.(μ-OH)(OTf)$_2$]** is larger compared to the starting complex, due to the electrostatic repulsion between the two Cu(II) ions but is in the range of other reported (μ-phenoxo)(μ-OH) dicopper complexes[25] and shorter compared to a bis(μ-thiophenolate) dinuclear compound.[26] For the two metal centers, the geometry can be described as nearly ideal tetragonal with τ values for Cu_1 and Cu_2 of 0.041 and 0.038 respectively. This structure, with a heterodiatomic doubled bridged {Cu_2(μ-S)(μ-OH)} core constitutes to the best of our knowledge, a unique example of such an arrangement for a dicopper system. Furthermore, as observed in the bulk mixture at the end of the reaction, this compound is EPR-silent in acetone. It also exhibits identical UV-Vis and electrochemical properties compared to the bulk mixture upon N_2O reduction.

Spectroscopic, kinetic and theoretical studies were then performed to get mechanistic insights. *First*, UV-visible and EPR showed the complete conversion of the starting material to the final **[3.(μ-OH)(OTf)$_2$]** species, as evidenced by the identical extinction coefficient of the 420 nm band characteristic of isolated **[3.(μ-OH)(OTf)$_2$]**. As the full conversion of the starting material is accompanied by the release of 0.4 eq. of N_2, a 0.5 N_2O / **[2.(H$_2$O)(OTf)]$^+$** stoichiometry for the reaction was determined. It reflects the fact that two electrons are required for N_2O reduction.

Second, the existence of a reaction intermediate was evidenced using ^{19}F NMR and electrochemistry. At the early stage of the reaction (*i.e.* slight changes in the hyperfine structure of the EPR spectrum compared to the starting material), a new signal was observed at -77.3 ppm that differs from the starting MV (-73.3 ppm) and the final μ-hydroxo (-77.9 ppm) species (Fig **11**).

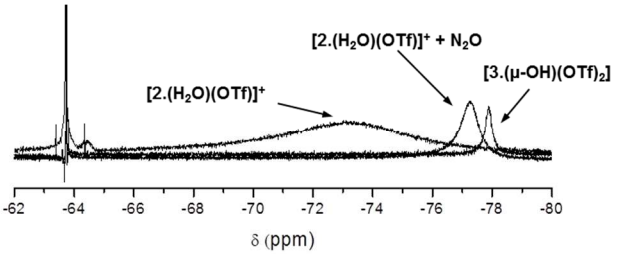

Fig 11. ^{19}F NMR spectra (acetone-d_6) for the starting **[2.(H$_2$O)(OTf)]$^+$** , **[2.(H$_2$O)(OTf)]$^+$** + N_2O (early stage of the reaction) and the final **[3.(μ-OH)(OTf)$_2$]** species. The peak at -63.73 ppm refers as the internal standard.

The -77.3 ppm signal is sharper compared to the starting complex, but still broader compared to the final μ-hydroxo compound. The triflate(s) ion(s) exchange process regime evidenced for the starting complex has then been modified, arguing for changes occurring in their close environment. One possibility is that N_2O competes with the water molecule at the copper coordination sphere and that this phenomenon affects the whole molecule. No shifts were observed when using **[1]** in a similar experiment. Independently, the evolution of the CV recorded from the open circuit potential of **[2.(H$_2$O)(OTf)]$^+$** (Fig. **12**, trace **(A)**), through the early stage of the reaction (N_2O bubbling with no EPR changes **(**trace **B)**) and after 12 minutes when the complex is formed **(**trace **C)** also indicate an interaction between the complex and the substrate. The profile of trace **(B)** resembles the one obtained in the presence of excess triflate (Fig. S14), but with a larger shift for the $Cu^{II}Cu^{I}/Cu^{II}Cu^{II}$ redox system from 417 to 270 mv (ΔE =148 mV). The CV curve starting from the open circuit potential (whatever the scan direction) in **(B)** indicates that the MV character of the complex is conserved at this stage of the reaction. The $Cu^{I}Cu^{I}/Cu^{II}Cu^{I}$ system is not affected while the $Cu^{II}Cu^{I}/Cu^{II}Cu^{II}$ one shifts towards more reductive potentials. As discussed in the solution studies section, we propose that ligand exchange occurs at the Cu center coordinated by the water molecule. As only N_2O is present as an extra molecule in the reaction mixture, this result enforces its coordination at the MV center. Then, the final product **[3.(μ-OH)(OTf)$_2$]** was observed after 12 minutes. No shift occurred in the case of **[1]** in a similar experiment, confirming the ligand exchange process presented for **[2.(H$_2$O)(OTf)]$^+$**.

All together, these data are consistent with N_2O binding at the dicopper center, and more than likely in place of the water molecule.

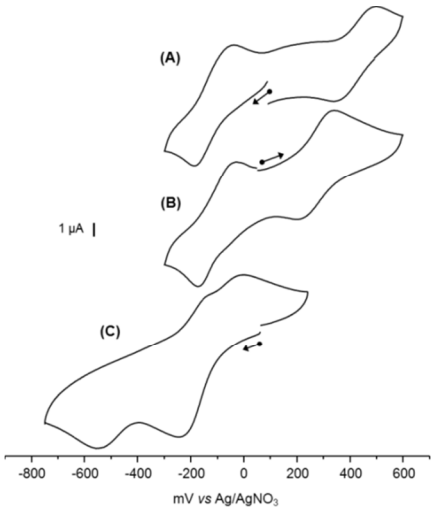

Fig 12. Evolution of the electrochemical behavior of **[2.(H_2O)(OTf)]$^+$** upon N_2O bubbling in acetone. **(A)** Starting material; **(B)** Early stage of the reaction and **(C)** After completion of the reaction (12 min). Experimental conditions: acetone + 0.1M $(nBu)_4NClO_4$ *vs.* $Ag/Ag(NO_3)$ (0.01 M in 0.1 M $(nBu)_4NClO_4$) with glassy carbon disk as working electrode at 100 $mV.s^{-1}$.

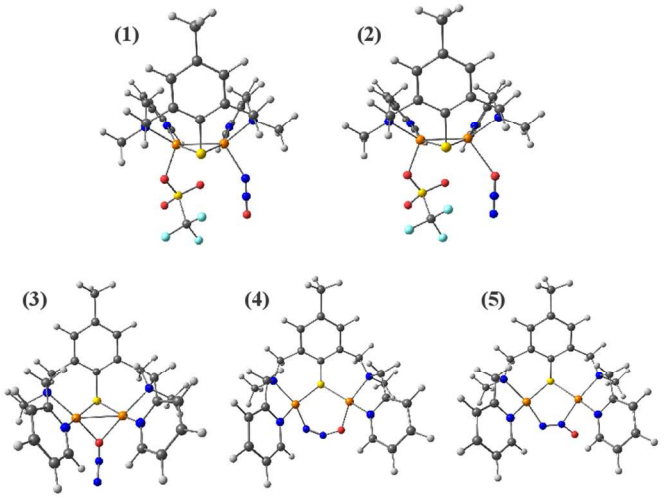

Fig. 13 Possible intermediates generated upon N_2O reaction with **[2.(H_2O)(OTf)]$^+$.**

Third, the reaction rate order *a* related to **[2.(H_2O)(OTf)]$^+$** species was determined under *pseudo* first-order conditions (excess N_2O, eqs (1) and (2), Fig. S20 and S21). A *a* value of 0.9 ± 0.1 was obtained while plotting lnk' as a function of ln**[2.(H_2O)(OTf)]$^+$**. This result excludes a direct conversion of N_2O by 2 molar equiv. of **[2.(H_2O)(OTf)]$^+$** required for a concerted mechanism. In this case, a rate order of two should have been obtained.

$$a[2.(H_2O)(OTf)] + bN_2O \xrightarrow{k1} Prod + N_2 \quad (1)$$

$$v = k1[2.(H_2O)(OTf)]^a[N_2O]^b = k'[2.(H_2O)(OTf)]^a \quad with\ k' = k1[N_2O]^b \quad (2)$$

Consequently, the kinetic data led us to consider a rate limiting step coming from coupled reaction involving an intermediate that consumes the starting complex. A second order rate constant of 0.03 ± 0.001 $M^{-1}.s^{-1}$ was estimated under atmospheric N_2O pressure. Moreover, the displacement of the water molecule in the reaction pathway was also evidenced: upon addition of one equivalent of DABCO to an acetone solution of **[2.(H_2O)(OTf)]$^+$**, the resulting hydroxo-containing complex exhibited no reactivity towards N_2O (Fig. S22). This result indicates that the presence of a stronger ligand in the metal coordination sphere prevents N_2O coordination. The reaction was also inhibited by the presence of excess triflate but to a lesser extent.

N_2O binding at the copper complex has finally been investigated by theoretical calculations. The reaction of **[2.(H_2O)(OTf)]$^+$** with N_2O lead us to consider five possible adducts resulting from N_2O binding at the $\{Cu_2S\}$ core (Fig. **13**).

(1) and **(2)** correspond to ligand exchange between the water molecule of **[2.(H_2O)(OTf)]$^+$** and N_2O. In these structures, N_2O binds in a monodentate way to only one copper center, through the nitrogen or the oxygen atom. The three other adducts correspond to the coordination modes involving both copper ions. Upon geometry optimization, the electronic structures of the five adducts were computed along with the prediction of their respective absorption spectra (Fig. S23). Since the follow-up of the reaction by UV-Vis showed an isosbestic point and that EPR does not indicate the presence of new features compared to the starting complex, we suggest that the N_2O-adduct exhibits spectroscopic properties close to that of **[2.(H_2O)(OTf)]$^+$**. Based on the DFT results, only **(1)** and **(2)**, featuring either a linear η^1-N or η^1-O N_2O, possesses a fully delocalized mixed-valent character together with a spectral signatures similar to that of **[2.(H_2O)(OTf)]$^+$**. The η^1-O analogue **(2)** has been estimated to be 2 kcal disfavored compared to **(1)**. The calculated UV-Vis spectrum of **(1)** remarkably resembles the one of **[2.(H_2O)(OTf)]$^+$** (Fig. **14**). According to the geometry-optimized structure (Fig. **14**, inset), the predicted Cu-Cu bond length of 2.58 angstroms is similar to that of **[2.(H_2O)(OTf)]$^+$** showing that the Cu-Cu bond remains even after N_2O binding. The spin density plot as well as the SOMO of this adduct are depicted in Fig. S24. **(1)** and **[2.(H_2O)(OTf)]$^+$** display similar spin distribution patterns which mainly involve the copper and sulfur atoms (0.20 on Cu_1, 0.28 on Cu_2 and 0.23 on S). The SOMO **(1)** is also consistent with a σ antibonding interaction between the metal and the sulfur orbitals.

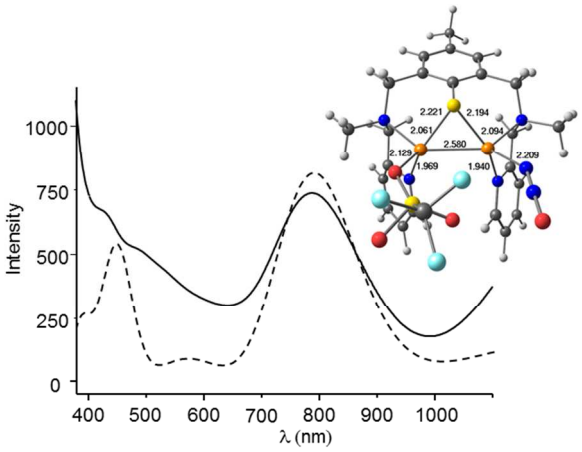

Fig. 14 UV-Vis spectra of **[2.(H$_2$O)(OTf]** (solid line) in acetone and of the calculated (dotted line) **(1)**. Inset: geometry-optimized structure for **(1)**, with selected bond lengths.

Several reaction pathways can be envisaged but all are initiated by N_2O binding, involving an equilibrium between **[2.(H$_2$O)(OTf)]$^+$** and **[2.(N$_2$O)(OTf)]$^+$**, as evidenced above. The latter species (**(1)** or **(2),** scheme **2**) can either be directly reduced by the starting species to provide **[3.(μ-OH)(OTf)$_2$]**, or being reduced after N_2 evolution, to form intermediate **HV**, proposed as a high-valent copper (III,II) or a ligand-centered radical [Cu(II)Cu(II)L$^{\cdot}$] species. The first reaction is not thermodynamically favored due to the redox potentials observed for the intermediate (270 mV) compared to the starting complex (417 mV). Moreover, if the unique O-atom source was N_2O, the 0.5 N_2O / **[2.(H$_2$O)(OTf)]$^+$** ratio is not realistic since only 0.5 equiv. of the final **[3.(μ-OH)(OTf)$_2$]** compound should have been isolated. The consequence is that the oxygen atom for the other half of the final complex, together with the required proton come from the bimolecular reaction between **[2.(H$_2$O)(OTf)]$^+$** and intermediate **HV**. Given these results, a consistent reaction pathway can be proposed (Scheme **2**).

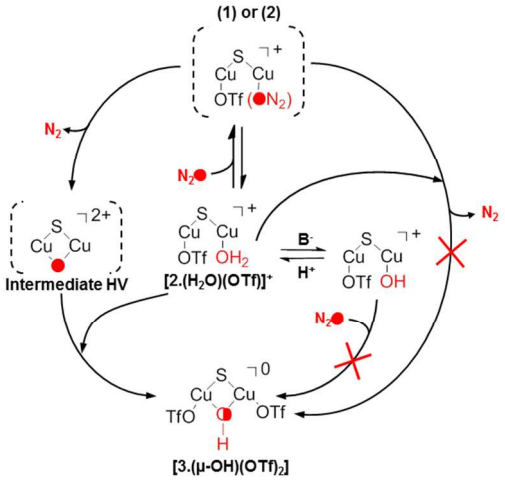

Scheme 2. Proposed reaction pathway for N_2O reduction by **[2.(H$_2$O)(OTf)]$^+$**.

Implications for N_2O Reductase mechanism

Our study demonstrates that the presence of labile sites (weak coordinating ligands) is required to provide N_2O reduction. This is in line with the high activity of N_2Or from *Marinobacter hydrocarbonoclasticus* which contains an open coordination site at the Cu_I-Cu_{IV} edge. In this case the binding of iodine causes an inhibition of the reactivity. Recent work reported by Solomon and co-workers also reached the same conclusion.[12a] In this case, the reactivity of the active site of N_2Or having an extra sulfide anion at the Cu_I-Cu_{IV} edge is impressively low. Our system has a second order rate constant of 0.01 ± 0.001 s^{-1} which is closer to Cu_Z^* (corresponding to the resting state of the enzyme containing an OH^-/OH_2 bridge) compared to Cu_Z under steady state conditions (S-containing active state). The interaction between N_2O with Cu_Z^* is yet to be fully established, but these results combined with previously reported research strongly suggests the presence of a N_2O-Cu_Z adduct. Interestingly, our study illustrates that N_2O binding does not dramatically affect the UV-visible (mainly displaying CT bands) and EPR spectra, but significantly alters the redox properties of our starting complex. Sophisticated spectroscopies are therefore required to confirm N_2O ligation in enzymes or inorganic complexes. Furthermore, the presence of an oxygen-based bridge in the final mimic complex is also relevant to a possible N_2O adduct prior to N_2 release (the oxygen atom originating from N_2O). Unfortunately, the absence of intermediate stabilization in our experimental conditions precludes its absolute demonstration at this time. However, we propose that the presence of such a ligand in the active reduced state of the enzyme is unlikely since in our case the reactivity is fully inhibited. Finally, the observed Cu-O(H)x distance in the X-ray crystal structure of Cu_Z center from the pink form of *Achromobacter cycloclastes* (2.14 Å) is comparable with that of the hydroxide bond to our complex, giving our novel complex particular structural relevance.

Conclusion

A new type of MV dicopper species with two different exchangeable ligands at the metal centers has been fully characterized. Spectroscopic, electrochemical and theoretical studies indicate that the predominant species in solution is identical to the complex characterized by X-ray crystallography. Interestingly, the electronic properties of this species are not representative of its dissymmetry. This complex is capable of N_2O reduction, as illustrated by N_2 release. Once again, a combination of experimental and theoretical considerations helped in providing a realistic reaction pathway, as well as allowing the proposal of a structure consistent with an N_2O bound adduct. We have unequivocally proven the labile water molecule to be essential for the reactivity. Even if our system is non-catalytic, our study illustrates that a bio-inspired approach remains a valuable strategy for the design of accurate molecules capable of N_2O activation. Additional

experiments are in progress in our lab to identify metal-based intermediates.

Acknowledgments

The authors gratefully acknowledge the Labex ARCANE ANR-11-LABX-0003-01, the CNRS, CEA and the University of Grenoble-Alpes for supporting this work. We thank Dr J. M. Latour for fruitful discussion during the writing of the manuscript, Dr L. Dubois for his assistance in recording solid state UV-Vis NIR spectra and Dr T. Simmons for his careful reading of the manuscript.

References

1. S. Solomon, D. Qin, M. Manning, Z. Chen, M. Marquis, K. Averyt, M. M. B. Tignor and H. L. Miller, *Contribution of Working Group I to the fourth Assessment report of the Intergovernmental Panel on climate Change, 2007;*, Cambridge University Press: Cambridge, UK, 2007.
2. A. R. Ravishankara, J. S. Daniel and R. W. Portmann, *Science*, 2009, **326**, 123-125.
3. V. A. Samarkin, M. T. Madigan, M. W. Bowles, K. L. Casciotti, J. C. Priscu, C. P. McKay and S. B. Joye, *Nature Geosci*, 2010, **3**, 341-344.
4. A. Leont'ev, O. g. Fomicheva, M. Proskurnina and N. Zefirov, *Russ. Chem. Rev.*, 2001, **70**, 91-104.
5. D. J. Xiao, E. D. Bloch, J. A. Mason, W. L. Queen, M. R. Hudson, N. Planas, J. Borycz, A. L. Dzubak, P. Verma, K. Lee, F. Bonino, V. Crocellà, J. Yano, S. Bordiga, D. G. Truhlar, L. Gagliardi, C. M. Brown and J. R. Long, *Nat Chem*, 2014, **6**, 590-595.
6. (a) E. K. Beloglazkina, A. G. Majouga, A. A. Moiseeva, N. V. Zyk and N. S. Zefirov, *Mendeleev Commun.*, 2009, **19**, 69-71; (b) R. Ben-Daniel, L. Weiner and R. Neumann, *J. Am. Chem. Soc.*, 2002, **124**, 8788-8789; (c) A. N. Chernysheva, E. K. Beloglazkina, A. A. Moiseeva, R. L. Antipin, N. V. Zyk and N. S. Zefirov, *Mendeleev Commun.*, 2012, **22**, 70-72; (d) J. Ettedgui and R. Neumann, *J. Am. Chem. Soc.*, 2009, **131**, 4-5; (e) H. Goldberg, D. Kumar, G. N. Sastry, G. Leitus and R. Neumann, *J. Mol. Catal. A: Chem.*, 2012, **356**, 152-157; (f) K. Hashimoto, Y. Kitaichi, H. Tanaka, T. Ikeno and T. Yamada, *Chem. Lett.*, 2001, **30**, 922-923; (g) K. Hashimoto, H. Tanaka, T. Ikeno and T. Yamada, *Chem. Lett.*, 2002, **31**, 582-583; (h) G. Kiefer, L. Jeanbourquin and K. Severin, *Angew. Chem. Int. Ed.*, 2013, **52**, 6302-6305; (i) H. Tanaka, K. Hashimoto, K. Suzuki, Y. Kitaichi, M. Sato, T. Ikeno and T. Yamada, *Bull. Chem. Soc. Jpn.*, 2004, **77**, 1905-1914; (j) A. G. Tskhovrebov, E. Solari, R. Scopelliti and K. Severin, *Organometallics*, 2012, **31**, 7235 - 7240; (k) T. Yamada, K. Hashimoto, Y. Kitaichi, K. Suzuki and T. Ikeno, *Chem. Lett.*, 2001, **30**, 268-269; (l) T. Yamada, K. Suzuki, K. Hashimoto and T. Ikeno, *Chem. Lett.*, 1999, **28**, 1043-1044.
7. S. Dell'Acqua, S. Pauleta, P. Paes de Sousa, E. Monzani, L. Casella, J. Moura and I. Moura, *J. Biol. Inorg. Chem.*, 2010, **15**, 967-976.
8. P. Chen, S. I. Gorelsky, S. Ghosh and E. I. Solomon, *Angew. Chem. Int. Ed.*, 2004, **43**, 4132-4140.
9. S. Ghosh, S. I. Gorelsky, S. DeBeer George, J. M. Chan, I. Cabrito, D. M. Dooley, J. J. G. Moura, I. Moura and E. I. Solomon, *J. Am. Chem. Soc.*, 2007, **129**, 3955-3965.
10. (a) K. Brown, K. Djinovic-Carugo, T. Haltia, I. Cabrito, M. Saraste, J. J. G. Moura, I. Moura, M. Tegoni and C. Cambillau, *J. Biol. Chem.*, 2000, **275**, 41133-41136; (b) K. Brown, M. Tegoni, M. Prudencio, A. S. Pereira, S. Besson, J. J. Moura, I. Moura and C. Cambillau, *Nat Struct Mol Biol*, 2000, **7**, 191-195; (c) T. Haltia, K. Brown, M. Tegoni, C. Cambillau, M. Saraste, K. Mattila and K. Djinovic-Carugo, *Biochem. J.*, 2003, **369**, 77-88; (d) K. Paraskevopoulos, M. Sundararajan, R. Surendran, M. A. Hough, R. R. Eady, I. H. Hillier and S. S. Hasnain, *Dalton Trans.*, 2006, 3067-3076.
11. A. Pomowski, W. G. Zumft, P. M. H. Kroneck and O. Einsle, *Nature*, 2011, **477**, 234-237.
12. (a) E. M. Johnston, S. Dell'Acqua, S. Ramos, S. R. Pauleta, I. Moura and E. I. Solomon, *J. Am. Chem. Soc.*, 2014, **136**, 614-617; (b) S. R. Pauleta, S. Dell'Acqua and I. Moura, *Coord. Chem. Rev.*, 2013, **257**, 332-349.
13. S. I. Gorelsky, S. Ghosh and E. I. Solomon, *J. Am. Chem. Soc.*, 2006, **128**, 278-290.
14. A. Wust, L. Schneider, A. Pomowski, W. G. Zumft, P. M. H. Kroneck and O. Einsle, *Biol. Chem.*, 2012, **393**, 1067-1077.
15. (a) I. Bar-Nahum, J. T. York, V. G. Young and W. B. Tolman, *Angew. Chem. Int. Ed.*, 2008, **47**, 533-536; (b) E. C. Brown, N. W. Aboelella, A. M. Reynolds, G. Aullon, S. Alvarez and W. B. Tolman, *Inorg. Chem.*, 2004, **43**, 3335-3337; (c) E. C. Brown, I. Bar-Nahum, J. T. York, N. W. Aboelella and W. B. Tolman, *Inorg. Chem.*, 2007, **46**, 486-496; (d) E. C. Brown, J. T. York, W. E. Antholine, E. Ruiz, S. Alvarez and W. B. Tolman, *J. Am. Chem. Soc.*, 2005, **127**, 13752-13753; (e) P. Chen, K. Fujisawa, M. E. Helton, K. D. Karlin and E. I. Solomon, *J. Am. Chem. Soc.*, 2003, **125**, 6394-6408; (f) M. E. Helton, P. Chen, P. P. Paul, Z. Tyeklár, R. D. Sommer, L. N. Zakharov, A. L. Rheingold, E. I. Solomon and K. D. Karlin, *J. Am. Chem. Soc.*, 2003, **125**, 1160-1161; (g) M. E. Helton, D. Maiti, L. N. Zakharov, A. L. Rheingold, J. A. Porco and K. D. Karlin, *Angew. Chem. Int. Ed.*, 2006, **45**, 1138-1141; (h) Y. Lee, A. A. N. Sarjeant and K. D. Karlin, *Chem. Commun.*, 2006, 621-623; (i) D. Maiti, J. S. Woertink, M. A. Vance, A. E. Milligan, A. A. Narducci Sarjeant, E. I. Solomon and K. D. Karlin, *J. Am. Chem. Soc.*, 2007, **129**, 8882-8892; (j) J. T. York, I. Bar-Nahum and W. B. Tolman, *Inorg. Chem.*, 2007, **46**, 8105-8107; (k) J. T. York, I. Bar-Nahum and W. B. Tolman, *Inorg. Chim. Acta*, 2008, **361**, 885-893.
16. I. Bar-Nahum, A. K. Gupta, S. M. Huber, M. Z. Ertem, C. J. Cramer and W. B. Tolman, *J. Am. Chem. Soc.*, 2009, **131**, 2812-2814.
17. S. Torelli, M. Orio, J. Pécaut, H. Jamet, L. Le Pape and S. Ménage, *Angew. Chem. Int. Ed.*, 2010, **49**, 8249-8252.
18. A. W. Addison, T. N. Rao, J. Reedijk, J. van Rijn and G. C. Verschoor, *J. Chem. Soc., Dalton Trans.*, 1984, **0**, 1349-1356.
19. (a) R. Gupta, Z. H. Zhang, D. Powell, M. P. Hendrich and A. S. Borovik, *Inorg. Chem.*, 2002, **41**, 5100-5106; (b) J. R. Hagadorn, T. I. Zahn, J. L. Que and W. B. Tolman, *Dalton Trans.*, 2003, **0**, 1790-1794; (c) S. Kababya, J. Nelson, C. Calle, F. Neese and D. Goldfarb, *J. Am. Chem. Soc.*, 2006, **128**, 2017-2029; (d) J. Kuzelka, S. Mukhopadhyay, B. Spingler and S. J. Lippard, *Inorg. Chem.*, 2004, **43**, 1751-1761; (e) D. D. LeCloux, R. Davydov and S. J. Lippard, *J.*

Am. Chem. Soc., 1998, **120**, 6810-6811; (f) D. D. LeCloux, R. Davydov and S. J. Lippard, *Inorg. Chem.*, 1998, **37**, 6814-6826.

20. J. Irangu, M. J. Ferguson and R. B. Jordan, *Inorg. Chem.*, 2005, **44**, 1619-1625.
21. aP. Day, N. S. Hush and R. J. H. Clark, *Phil. Trans. R. Soc. A*, 2008, **366**, 5-14; bM. Robin and D. Peter, *Adv. Inorg. Chem. Radiochem*, 1967, **10**, 247-422.
22. D. R. Gamelin, D. W. Randall, M. T. Hay, R. P. Houser, T. C. Mulder, G. W. Canters, S. de Vries, W. B. Tolman, Y. Lu and E. I. Solomon, *J. Am. Chem. Soc.*, 1998, **120**, 5246-5263.
23. S. Chardon-Noblat, O. Horner, B. Chabut, F. Avenier, N. Debaecker, P. Jones, J. Pécaut, L. Dubois, C. Jeandey, J.-L. Oddou, A. Deronzier and J.-M. Latour, *Inorg. Chem.*, 2004, **43**, 1638-1648.
24. R. P. Houser, V. G. Young and W. B. Tolman, *J. Am. Chem. Soc.*, 1996, **118**, 2101-2102.
25. (a) C. Belle, C. Beguin, I. Gautier-Luneau, S. Hamman, C. Philouze, J. L. Pierre, F. Thomas and S. Torelli, *Inorg. Chem.*, 2002, **41**, 479-491; (b) S. Torelli, C. Belle, I. Gautier-Luneau, J. L. Pierre, E. Saint-Aman, J. M. Latour, L. Le Pape and D. Luneau, *Inorg. Chem.*, 2000, **39**, 3526-3536.
26. W. Rammal, C. Belle, C. Beguin, C. Duboc, C. Philouze, J. L. Pierre,L. Le Pape, S. Bertaina, E. Saint-Aman and S. Torelli, *Inorg. Chem.*, 2006, **45**, 10355-10362.

